ISSN: 2578-7365

Research Article

Journal of Chemistry: Education Research and Practice

Synthesis and Structural Studies on some Dioxomolybdenum (VI) Complexes Bearing 1-(1-Hydroxynaphthalen-2-yl) Ethanone Moiety

Mohammad S El-Shahawi1*, Mai Mostafa A Hassan Shanab2, Mohsen M Mostafa3

[1]*Department of Chemistry, Faculty of Science, King Abdul-Aziz University, P. O. Box 80203, Jeddah 21589, Saudi Arabia*

[2]*Department of Chemistry, Science and Humanity Studies College–Prince Sattam Bin Abdul-Aziz University, P.O. Box: 13 Hawtat Bani Tamem 11149, Saudi Arabia*

[3]*Department of chemistry, Faculty of Science, Mansoura University, Egypt*

***Corresponding author**

Mohammad S El-Shahawi, Department of Chemistry, Faculty of Science, King Abdul-Aziz University, P.O.Box 80203, Jeddah 21589, Saudi Arabia, E-mail: mohammad_el_shahawi@yahoo.co.uk

Submitted: 07 June 2019; **Accepted**: 12 June 2019; **Published**: 28 June 2019

Abstract

A number of new molybdenum complexes Cis-$MoO_2(NE)_2.CH_3OH$, Cis-$MoO_2(HRSB)_2.nH_2O$ {R= H, 4-Br, 4-OCH_3, 4-CH_3 and n= 0, 1, 2} Cis-$MoO_2(HL)(acac).nH_2O$ {HL= HNEBH, HNEINH, HNENH, HNEPH, n=0, 1}, Cis-$[MoO_2(L\)_2.nH_2O]$, {L\= HNE-2-ABH, HNE-4-ABH, n = 0, 2} and Cis-$[Mo_2O_5(HNEAH)_2]$ have been synthesized and characterization by magnetic, spectroscopic (FT-IR, 1H and 13C-NMR spectra) and electrochemical techniques. The complexes were made reaction of Cis-$MoO_2(acac)_2$ with the ligands, (1-hydroxynaphthalen-2-yl)ethenone (HNE), (E)-2-(1-(phenylimino)ethyl)naphthalen-1-ol (HASB), (E)-2-(1-(p-tolylimino)ethyl) naphthalen-1-ol (HTSB), E-2-(1-(4-methoxyphenylimino)ethyl)naphthalen-1-ol (HMSB) and (E)-2-(1-(4-bromophenylimino)ethyl)naphthalen-1-ol (HBrSB) monobasic bidentate (NO) or 2-anmino-N/-(1-(1-hydroxynaphthalene-2-yl)ethylidene)benzohydrazide (HNE2-ABH), 4-anmino-N/-(1-(1-hydroxynaphthalene-2-yl) ethylidene)benzohydrazide (HNE4-ABH), N/-(1-(1-hydroxynaphthalene-2-yl)ethylidene)benzohydrazide (HNEBH), N-(1-(1-hydroxynaphthalene-2-yl)ethylidene)acetohydrazide (HNEAH), N/-(1-(1-hydroxynaphthalene-2-yl)ethylidene) nicotinohydrazide (HNENH), N/-(1-(1-hydroxynaphthalene-2-yl)ethylidene)isonicotinohydrazide (HNEINH), N/-(1-(1-hydroxynaphthalene-2-yl)ethylidene)picolinohydrazide (HNEPH), they coordinate as dibasic tridentate (OON). Both the molecular and the spectroscopic studies showed that, the complexes are octahedrally coordinated. The redox properties, of the electrode couples and the stability of some complexes towards reduction were linked to the electron withdrawing or ability releasing of the substituent in the Schiff bases and the hydrazones. Results show that, changes in $E_{1/2}$ for the complexes due to remote substituent effects could be related to changes in basicity of the carbonyl oxygen of the hydrazide moiety in the hydrazone ligand. The electron-donating substituents stabilized Mo(VI) complexes while electron-withdrawing groups favored lower oxidation state of Mo(V) and/ or Mo(IV) species. The nature of mechanism and kinetic parameters of the electroactive chelates are strongly dependent on the substituent. The E_{HOMO} and E_{LUMO} level, of hydrazone and some of Cis-molybdenum complexes, from both electrochemical and theoretical data also back-donation energy ($\Delta E_{back\text{-}donation}$), ionization potential (I), molecular dipole moment (μ), electronegativity (χ), softness (σ) electron affinity (A), global hardness (η), and electrophilicity index (ω) were calculated.

Keywords: Molybdenum (VI) Complexes; Cyclic Voltammetry; Schiff base; DFT

Introduction

Last decades have seen an escalation of interest in the applications of spectroscopic and electroanalytical techniques to study the oxidation and reduction reaction of many types of chelating agents and their metal chelates [1-12]. Hydrazones or Schiff bases derived from 1-(1-hydroxynaphthalen-2-yl)ethanone (HNE), have flexible fashion, which coordinated to a metal ion through α- hydroxynaphthalene, imine nitrogen atom of hydrazone moiety and the protonated / deprotonated amide oxygen atom, the additional donor atom (N or O) forming chelating colored compounds [1,6,13,14].

Also, the molybdenum becomes fascinating in recent research due to presence of molybdenum in metalloenzymes and its catalytic activity of epoxidation of alkene [15]. Hitherto no data have been reported on molybdenum (VI) complexes of the 1-(1-hydroxynaphthalen-2-yl)ethanone (HNE) and its hydrazone Schiff base ligands. We have reported herein the synthesis, geometry, redox properties, nature and mechanism of the electrode couples of some novel molybdenum (VI) chelates in solid state. The complexes of potential multi dentate Schiff bases provide good opportunity for investigating the azomethine nitrogen and hydroxyl oxygen coordination in a bi-dentate (ON) fashion. The possibility of keto-enol tautomerism of the >C=N-NH-C=O to >C=N-N=C-OH moiety may control the bonding and the stereo chemical behavior of the prepared complexes.

Experimental

Materials and Reagents

The reagent 1-(1-hydroxynaphthalen-2-yl) ethenone (HNE), acetylacetone (acac), tetrabutylammonium tetrafluoroborate (TBA^+BF4^-) as supporting electrolyte and N,N-dimethylformamide (DMF) were supplied from BDH and were used as received. The analytical data of the prepared hydrazones Schiff bases are given in Table 1 whereas the chemical formulae are shown in Fig. 1. The complex *Cis*-$MoO_2(acac)_2$ was prepared by the method reported by Chen, et al [16]. Other chemicals were used as analytical reagent grade.

Physical measurements

Infrared spectra measurements (200-4000 cm^{-1}) of the ligands and their molybdenum (VI) complexes as KBr discs and as a mull in liquid paraffin between NaCl plates were measured on a Mattson 5000 FTIR Spectrophotometer. ^{13}C, ^{1}H-NMR and the electronic spectra of the ligands and their molybdenum complexes in DMF or DMSO were recorded on $UV_{2\text{-}100}$ Unicom UV/vis and a Varian EM-390 MHz Spectrophotometers, respectively. The cyclic voltammetry measurements were carried out on a potentiostat wave generator (Oxford press) equipped with a Phillips PM 8043 X-Y recorder. The electrode assembly consists of platinum wires of 0.5 mm diameter as working and counter electrodes and Ag/AgCl as a reference electrode. The magnetic data were measured on a Johnson-Matthey magnetic susceptibility balance. Carbon, hydrogen and nitrogen content was determined at the Micro analytical Unit at Cairo University, Egypt. Molybdenum content was determined gravimetrically as $PbMoO_4$ [17].

Computational details

Gaussian software was used in calculation Gauss. View 6.0.8 program [18]. Optimizations of geometrical the singlet ground state of the hydrazones using DFT at B3LYP-6-311G level and molybdenum complexes base set BPV86 hybrid [19]. The optimization was confirmed by the absence of negative frequency.

Preparation of the Schiff bases (HRSB) and hydrazones

The Schiff bases were made according the preceduge reported in the literature [20]. The Schiff bases and hydrazones ligands (Fig. 1) were prepared by mixing equimolar quantities of 1-(1-hydroxynaphthalen-2-yl)ethanone (HNE) with aniline and substituted anline, hydrazine and substituted in ethanol. Each reaction mixture was refluxed for 3h with contenous stirring. On concentrating the solutions and cooling, polycrystalline yellow colored precipitates were separated out, filtered off, washed with ethanol, diethylether, recrystallised from ethanol and finally dried in vacuum. Most of these chelates are shiny yellow to orang crystal colored and have melting point below 235 °C.

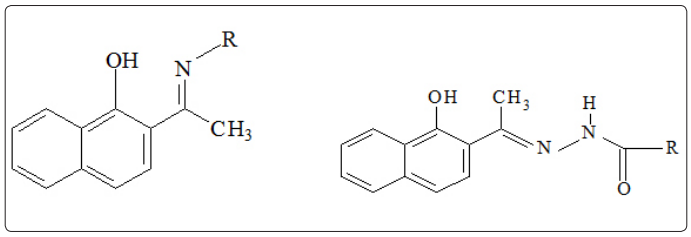

R = C_6H_5 (HBSB)

R= 4-BrC_6H_4 (HBrSB)

R= 4-$OCH_3C_6H_4$ (HMSB)

R= 4-$CH_3C_6H_4$ (HTSB)

R = C_6H_5 (HNEBH)

R = 2\-$NH_2C_6H_4$ (HNE-2\-ABH)

R = 4\-$NH_2C_6H_4$ (HNE-4\-ABH)

R = CH_3 (HNEAH)

R = C_5H_4N (HNEINH

R = C_5H_4N (HNENH)

R = C_5H_4N (HNEPH)

Figure 1: General formulae of the ligands derivatives from Schiff bases (a) Hydrazones(b).

Preparation of Cis-molybdenum complexes

An accurate weight of the complex *Cis*-$MoO_2(acac)_2$, (1 mmol) in methanol (20 cm^3) was refluxed with the appropriate weight of the reagent HNE, Schiff bases or hydrazones (2 mmol) in methanol. The produced precipitates were separated out, filtered off, washed with hot methanol, diethylether, dried under vacuum and finally stored in a desiccator over anhydrous $CaCl_2$.

Results and discussion

The molybdenum(VI) complexes, *Cis*-$MoO_2(NE)_2.CH_3OH$, *Cis*-$MoO_2(HRSB)_2.nH_2O$ {R= H, 4-Br, 4-OCH_3, 4-CH_3 (Fig. 1. a) and n= 0, 1, 2 *Cis*-$MoO_2(HL)(acac).nH_2O$ {HL= HNEBH, HNEINH, HNENH, HNEPH (Fig.1.b), n=0, 1}, *Cis*-$[MoO_2(L)2.nH_2O]$, (L= HNE-2-ABH, HNE-4-ABH, n = 0, 2) and *Cis*-$[Mo_2O_5(HNEAH)_2]$ were prepared by a procedure similar to that reported for molybdenum (VI) complexes [21]. The isolated complexes are listed in Table 1 together with their analytical data and physical properties.

The solid complexes are colored and the proposed chemical structures of the complexes are in good agreement with the stoichiometries concluded from their analytical data (Table 1). The prepared complexes are stable at room temperature and are soluble in common organic solvents like, $CHCl_3$, CH_2Cl_2 and DMF. The conductivity measurements showed the non-electrolytic properties of these complexes [22]. Magnetic susceptibility measurements showed diamagnetic behaviour of all the complexes at room temperature as expected for dioxomolybdenum (VI) [12].

Results and discussion

The molybdenum(VI) complexes, *Cis*-$MoO_2(NE)_2.CH_3OH$, *Cis*-$MoO_2(HRSB)_2.nH_2O$ {R= H, 4-Br, 4-OCH_3, 4-CH_3 (Fig. 1. a) and n= 0, 1, 2 *Cis*-$MoO_2(HL)(acac).nH_2O$ {HL= HNEBH, HNEINH, HNENH, HNEPH (Fig.1.b), n=0, 1}, *Cis*-$[MoO_2(L)_2.nH_2O]$, (L= HNE-2-ABH, HNE-4-ABH, n = 0, 2) and *Cis*-$[Mo_2O_5(HNEAH)_2]$ were prepared by a procedure similar to that reported for molybdenum (VI) complexes [21]. The isolated complexes are listed in Table 1 together with their analytical data and physical properties.

The solid complexes are colored and the proposed chemical structures of the complexes are in good agreement with the stoichiometries concluded from their analytical data (Table 1). The prepared complexes are stable at room temperature and are soluble in common organic solvents like, $CHCl_3$, CH_2Cl_2 and DMF. The conductivity measurements showed the non-electrolytic properties of these complexes [22]. Magnetic susceptibility measurements showed diamagnetic behaviour of all the complexes at room temperature as expected for dioxomolybdenum (VI) [12].

Table 1: Physical properties and analytical data of molybedenum (VI) complexes of 1-(1-hydroxynaphthalen-2-yl)ethanone and Schiff base hydrazones

No.	Complex	Colour	m.p., °C	A_m*	Calculated (Found) %			
					C	H	N	M
1	$MoO_2(NE)_2.CH_3OH$	Yellow	285	1.1	56.6 (56.8)	4.2 (4.2)	__	18.1 (17.9)
2	$MoO_2(HBSB)_2.2H_2O$	Yellow	>300	11	63.2 (63.1)	4.7 (4.5)	4.1 (4.1)	14.0 (13.9)
3	$MoO_2(HBrSB)_2.H_2O$	Yellow	>300	2.1	52.5 (52.4)	3.4 (3.4)	3.4 (3.4)	11.6 (12.0)
4	$MoO_2(HMSB)_2.2H_2O$	Yellow	>300	3.2	61.3 (61.4)	4.9 (4.5)	3.8 (3.2)	12.9 (13.0)
5	$MoO_2(HTSB)_2$	Yellow	>300	1.2	67.5 (67.4)	4.8 (4.7)	4.1 (4.1)	14.2 (14.0)
6	MoO_2(HNEINH)(acac)	Orange	295	4.5	52.0 (51.7)	4.0 (4.1)	7.9 (7.9)	18.1 (18.1)
7	MoO_2(HNENH)(acac)	Orange	>300	5.1	52.0 (51.7)	4.0 (4.1)	7.9 (7.9)	18.1 (18.1)
8	MoO_2(HNEPH)(acac)	Orange	>300	6.1	52.0 (51.2)	4.0 (4.2)	7.9 (7.8)	18.1 (18.1)
9	Mo_2O_5(HNEAH)2	Brick-red	>300	6.9	44.6 (44.5)	3.5 (3.5)	7.4 (7.4)	25.4 (25.6)
10	MoO_2(HNEBH)(acac).H_2O	Brick-red	>300	9.5	44.6 (44.5)	3.5 (3.5)	7.4 (7.4)	25.4 (25.6)
11	MoO_2(HNE-2\-ABH)$_2$	Red	290	12.0	59.7 (59.1)	4.2 (3.5)	11.0 (11.0)	12.6 (12.1)
12	MoO_2(HNE-4\-ABH)$_2.2H_2O$	Yellow	>300	5.8	57.0 (56.6)	4.5 (3.9)	10.5 (10.5)	12.0 (12.1)

* in DMF Ω^{-1} cm^2 mol^{-1}

IR spectra

The characteristic IR spectral data of the ligands HNE, Schiff bases, and their molybdenum complexes are summarized in Table 2, along with their tentative assignments. The assignments of the IR bands of the complexes have been determined by careful comparison with the IR spectra of the free ligand and similar complexes [21]. The IR spectrum of the free HNE ligand, the broad band observed at 3423 cm^{-1}, is possibly attributed to the hydrogen bonding between hydroxy group of naphthyl and the oxygen of the acetyl group in ortho position [23]. The deformation vibration mode, δ(OH) observed at 1326 cm^{-1} in the spectrum of the ligand was not observed in the IR spectrum of Cis-$MoO_2(NE)_2.CH_3OH$. The vibration mode *ν*(C=O) observed at 1623cm^{-1} is shifted to lower wavenumber (~28 cm^{-1}) in the complex. These data suggest coordination of both OH and carbonyl oxygen atoms of the reagent HNE to the metal ions. Similar results have been reported in naphthalene-2,3-diolato and catecholato complexes [24,25]. The band observed at 1276 cm^{-1} in the free HNE ligand due to *ν*(C-O) is also shifted to lower wavenumber upon coordination [26-28]. These data emphasizes participation of the OH group upon coordination. The medium band observed at 1146 cm^{-1} arised from skeletal vibration modes of naphthalene ring in good agreement with the data reported for naphthalene-2, 3-diolato complexes [27].

The IR spectra of the solid Schiff bases(HRSB) derived from aniline and its 4-Br, 4-CH_3 and 4-OCH_3 derivatives showed a broad band in the range 3400-3300 cm^{-1} attributed to the interamolecular hydrogen-bonded naphtholic hydroxyl group [29,30]. The disappearance of this band in the spectra of their molybdenum complexes suggests the deprotonation of the naphtholic group and subsequent coordination of the hydroxyl oxygen to the metal ion [25,31]. In the spectra of the free Schiff bases (HRSB), the observed band in the range 1203-1275(s) cm-1, is ascribed to the naphthoyl *ν*(C-O) stretching vibration [32]. In the complexes of the Schiff bases this band is shifted to lower wavenumber in the region 1200-1269(m) cm^{-1} (Tables 2) suggesting that, the (C-O) group of the Schiff bases has taken part in the complex formation. The C=N, band in the range 1604-1629(s) cm^{-1} of the free Schiff bases HRSB (Table 2) is shifted to lower wavenumber region in the complexes, indicating participation of the azomethine nitrogen [33]. Thus, the Schiff bases HRSB are coordinated to the metal ions via the C=N nitrogen and the OH oxygen. This assignment is further supported by the appearance of new bands in the far IR at regions 1208-1255, 510-540 and 480 cm-1 due to the *ν*(C-O), *ν*(M-O), *ν*(M-N) vibrations, respectively [21].

Table 2: Vibration spectral data (cm^{-1}) of the prepared Schiff bases and their molybedenum (VI) chelates.*

No.	Compound	$\nu_{C=N}$ ($\nu_{C=O}$)	ν_{C-O}	ν_{C-C}	$\nu_{aromatic}$	δ_{OH}	ν_{M-O}	ν_{M-N}	ν_{s} MO_2	ν_{as} MO_2
1	HNE	1623(s)	1276(s)	1466(s)	1146(m)	1326(s)	—	—		
	$MoO_2(AN)_2.CH_3OH$	1614(m)	1248(m)	1450(s)	1154(m)	—	621(m)	—	938(s)	912
2	HBSB	1622(s)	1276(s)		—	1326(s)				
	$MoO(HBSB)_2.2H_2O$	1605(sh)	1215(m)	—			525(w)	430(w	919(m)	900(sh)
3	HBrSB	1619(s)	1276(s)	—	—	1325(s)				
	$MoO_2(HBrSB)2.H_2O$	1606(sh)	1225(m)	—	—		519(w)	422(w)	955(m)	919(sh)
4	HMSB	1623(s)	1277(s)		—	1386(m)				
	$MoO_2(HMSB)2.H_2O$	1619(sh)	1250(m)	—	—		522(m)	420(m)	950(s)	930(sh)
5	HTSB	1629(s)	1277(s)		—	1367(s)				
	$MoO_2(HTSB)_2$	1619(sh)	1250(m)	—	—	—	550(w)	420(w)	894(s)	894(m)

* s= strong, m = medium, w= weak, sh= shoulder and br=broad.

In the IR spectra of the complexes of the general formula *Cis*- $MoO_2(HRSB)_2.nH_2O$, (R= H, 4-Br, 4-CH_3, 4-OCH_3 and n= 1, 2), the lattice water is absorbed in the range 3200-3550 cm^{-1} due to the asymmetric and symmetric OH stretching [34,35]. The coordinated water normally showed the $p_r(H_2O)$ vibration at 887 cm^{-1} and $p_w(H_2O)$ near 553 cm^{-1} [32]. Thus, in the IR spectra of the molybdenum chelates, the two bands observed at 894 and 855 cm^{-1} and are safely assigned to the rocking vibration $p_r(H_2O)$ of the coordinated water confirming the coordination of water molecules [32,36].

The significant IR bands of the free hydrazone Schiff-base ligands and their related molybdenum complexes along with their probable assignments are given in Table 3. The IR bands of two hydrazone Schiff bases, HNEAH, HNEBH, and their molybdenum chelates are assigned by comparison with those of the free hydrazone Schiff bases and related complexes [36,37]. The IR spectra of the free Schiff bases showed three well defined bands at ca. 3440, 3380 and 2800 cm^{-1} and are safely assigned to ν_{as}(OH), ν_s(OH) and intramolecular hydrogen-bonded (OH) of naphtholic group, respectively [36]. A strong ν(NH) band centred in the 3203-3242 cm^{-1} regions was also observed. The observed bands in the region 1634-1663, 1568-1572 and 1327-1329 cm^{-1} are assigned to ν(C=O) of amide I, δ(NH) of amide II and ν(C-N) of amide III moieties, respectively, suggesting the existence of the two reagents in the keto form in the solid state [21,35-37]. The strong band observed in the region 1607-1633 cm^{-1} is assigned to ν(C=N) of the azomethine group [37].

Table 3: Vibration spectral data (cm-1) of the hydrazone Schiff bases (HNEAH and HNEBH) and their molybedenum (VI) chelates.*

Compound	ν(NH)	ν(C=O) Amide I	ν(C=N)	ν(N=CO)	ν(C-O)	ν(N-N)	νC-N	ν(M-O)	ν(M-N)	vs (MO_2)	vas (MO_2)
HNEBH	3203(s)	1634(s)	1607(sh)	---	---	857(s)	1367(s)	---	---	---	---
MoO_2(HNEBH) (acac).H_2O	—	—	1591(s)	1520(sh)	1323(s)	1094(m)	—	459(m)	322(m)	930(s)	950(sh)
HNEAH	3242(s)	1663(s)	1633(sh)	--	--	862(s)	1373(s)				__
$Mo_2O_5(HNEAH)_2$	__	__	1597(s)	1462(m)	1346(m)	1089(m)	__	490(w)	330(w)	851(s)	810(sh)

Compound	ν OH	vasNH2	vs NH2	νC=O	νC=N	ν(N=CO)	νC-O	νN-N	νC-N	νM-N	ν(MO)
HNE-2\-ABH	3471(s)	3360(s)	3207(s)	1622(s)	1600(sh)	____	____	956(m)	1385(s)	_____	___
MoO_2(HNE-2\-ABH)$_2$	3447(s)	3356(m)	__	__	1609(sh)	1576(s)	1327(s)	1096(m)	1384(s)	425(w)	344(w)
HNE-4\-ABH	3428(s)	3344(s)	3223(s)	1684(s)	1629(sh)	__	__	986(m)	1387(sh)	__	__
MoO_2(HNE-4\-ABH)2.$2H_2O$	3441(b)	3276(m)	__	__	1610(sh)	1586(s)	1296(m)	1087(m)	1370(s)	432(m)	350(w)

Compound	νOH	νNH	νC=O	ν C=N	ν(N=CO)	Pyridine ring vibrations				νN-N	νC-N
						I	II	III	VI		
HNEINH	3322(s)	3211(s)	1668(sh)	1626(s)	—	1600(sh)	1570(s)	1490	1410	978(m)	1386(s)
MoO_2(HNEINH) (acac)	3320(b)	—	—	1610(sh)	1548(s)	1600(s)	—	1460(m)	1414(m)	1049(m)	1381(m)
HNENH	----	3203(s)	1671(s)	1646(s)	—	1594((s)	1543(s)	1470(m)	1420(m)	951(s)	1391(m)
MoO_2(HNENH) (acac)	----	----	---	1600(s)	1547(s)	1582(s)	—	1458(m)	1414(sh)	1094(m)	1382(m)

HNEPH	3455(b)	3330(s)	1694(s)	1633(m)	__	1590(s)	1567(sh)	1467(m)	1428(m)	998(m)	1396(m)
MoO_2(HNEPH) acac)	3427(b)	—	—	1622(sh)	1525(m)	1580(s)	1550(m)	1460(m)	1393(m)	1334(m)	1024(m)

* s= strong, m = medium, w= weak, sh= shoulder and br=broad.

The two bands observed in the range 3200-3400 and 1636-1663 cm^{-1} due to *v*(NH) and *v*(C=O), respectively in the free ligands are disappeared in the spectra of the molybdenum complexes. On the other hand, a well-defined band near 1623 cm^{-1} due to *v*(C=N) was observed indicating that both -C=O and -NH groups are enolized and deprotonated in the complex formation with the tested metal ions [37]. Similarly, in the metal complexes the amide II bands of the free ligands were observed at lower wavenumbers (ca. 20 cm^{-1}) and the appearance of *v*(N=C-O) at ca. 1519 cm^{-1} and *v*(C-O) at ca. 1324 cm^{-1} were noticed confirming coordination of both Schiff bases to the metal ions through the deprotonated C-OH groups [28]. The *v*(N-N) of the free reagent was shifted to higher wavenumber (ca. 20 cm^{-1}) upon complex formation, confirming coordination of the azomethine nitrogen to the molydenum [21].

The existence of numerous coordination sites in the hydrazone ligands give variabl bonding modes. In the free hydrazone ligands HNE-2\-ABH and HNE-4\-ABH three bands in the range 3471-3428, 3360-3344, 3207-3223 cm-1 are observed and are safely assigned to *v*(OH), $v_{as}(NH_2)$ and v_{as}(NH) vibrations, respectively [38]. The two bands observed at 956 and 986 cm^{-1} in the free ligands are attributed to v_{as}(N-N) vibration[39] . The observed stretching vibration modes at 1684-1622 and 1629-1600 cm^{-1} are assigned to the *v*(C=O), and *v*(C=N) vibrations [38]. These data confirm the existence of the two hydrazones HNE-2\-ABH and HNE-4\-ABH in the keto form. The two broad bands at 2734 and 2600 cm^{-1} are safely assigned to O--H—NH stretching vibration and suggest the presence of intramolecular hydrogen bonding between the carbonyl oxygen and the amino groups [39].

A careful comparison of the IR spectra of the hydrazones and their molybdenum (VI) complexes indicated that, the two hydrazones coordinate to the metal ion in a bidentate and/or a tridentate manners. The Schiff base (HNE-2\-ABH) acts as a univalent bidentate ligand coordinating via the azomethine (C=N) nitrogen and the enol oxygen groups [40]. In the complexes of the general formulae, Cis-$[MoO_2(L)_2]$ where, L = HNE-2\-ABH; HNE-4\-ABH, the disappearance of both *v*(NH) and *v*(C=O); the shift of *v*(C=N) to lower (or higher) frequencies; the shift of *v*(N-N) to higher frequencies and finally the presence of the bands observed at 1337 and 1583 cm^{-1} due to δ(OH) and $\delta(NH_2)$, confirmed the participation of the carbonyl and azomethine groups in the coordination [41,42]. In the complexes, the disappearance of the IR band at 740 cm^{-1} due to δ(NH) out of plane, confirmed the participation of the two ligands in the enol form.

The spectra of the the Schiff bases (HL) HNEBH, HNEINH, HNENH, HNEPH ligands showed broad band in the range 3400-3445 cm^{-1} assigned to the *v*(OH) vibration mode [43]. In the IR spectra of their complexes *Cis*-$[MoO_2(HL)(acac).nH_2O]$ (where, n = 0, 1) this band was disappeared suggesting deprotonation and coordination of the hydroxyl group to the metal ion. The strong absorption bands in the range 1668-1694, 1626-1646, 1540-1518 cm^{-1} and 1329-1344 cm^{-1} of the hydrazones are assigned to *v*(C=O) amide-I, *v*(C=N) azomethine *v*(NH) amide-II and amide-III vibrations, respectively [13,44]. The observed bands in the regions 480-440(w) and 360-340(w) cm^{-1} in the metal chelates are tentatively assigned to *v*(M-O) and *v*(M-N), respectively [38,45,46]. The spectra of the complexes showed a bathochromic shift of the amide-I, -II and a hypsochromic shift of the amide-III bands suggesting participation of the carbonyl oxygen and the azomethine nitrogen in the complex formation. However, all the amide bands are totally disappeared from the spectra of the deprotonated molybdenum(VI) chelates, and a sharp diagnostic band for >C=N-N=C< group appeared in the range 1580-1595 cm^{-1}, suggesting formation of the carbonyl group in the enolic form through an amide to imidol toutomerism (Fig. 2) and subsequent coordination of the imidol oxygen upon deprotonation. The appearance of new characteristic bands of *v*(NCO-) at ~1500 and 1365 cm^{-1} added further support of the imidolic oxygen coordination to the metal ions [40,47]. The spectra of the dioxo-molybdenum(VI) complexes showed additional bands at 939 and 912 cm^{-1} due to the v_{as} MoO_2 and *v*s MoO_2 vibrations, respectively [48].

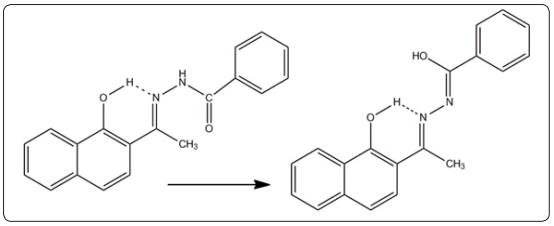

(a) (b)

Figure 2: Stracture of HENBH ligand (A) Keto form (B) enol form.

^{1}H-NMR spectra

The ^{1}H-NMR spectra of the free reagent HNE (Fig. 3 a) in $CDCl_3$ and d_6-DMSO, showed similar pattern accordance with the reported data the H_3 and H_8 protons, in the ortho position to the hydroxy and carbonyl groups appeared as a doublet at δ 8.4 and 7.2 ppm, respectively [49]. The H_4 and H_7 in the 4-position appeared at δ 7.7 and 7.4 ppm, respectively [49]. The proton of the hydroxy group appeared as a sharp signal at δ 14.05 ppm due to the hydrogen bonding and the ring current isotopic effect in the molecular structure [23,50]. The triplet band at δ 2.65 ppm is assigned to the methyl group protons [51].

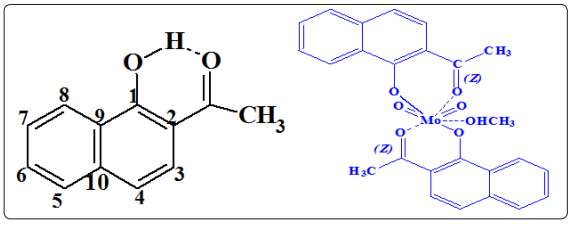

(a) (b)

Figure 3: atom numbering scheme of HNE (a) and *Cis*-$MoO_2(NE)_2CH_3OH$ complex (b)

In the ^{1}H-NMR spectrum of the complex, Cis-$[MoO_2(NE)_2CH_3OH]$ (Fig. 3 b) in d6-DMSO using TMS as an internal standard, the methyl protons in the 2- position to the carbonyl group are shifted to upfield

(~0.3 ppm), indicating participation of the C=O in coordination [52]. The deshielding due to the donation of the nonbonding electrons of the carbonyl oxygen atom to the molybdenum atom may account for such shift [44].

The hydroxy proton signal was not observed in the complex confirming replacement of the OH proton by the metal ion [53,54]. The observed signal at δ 1.71 ppm confirm the presence of methanol molecules in the coordination sphere of the complex.

^{1}H-NMR spectrum of the Schiff base HTSB showed a well-defined signal at δ = 14.0 ppm safely is assigned to hydroxyl group. The existence of the OH signal at high values downfield of TMS is due to the strong intramolecular hydrogen bonding between the OH and the azomethine group of Schiff base [43,55]. The observed signals at δ= 3.3-3.2 ppm with integration equivalent to three protons is assigned to the CH_3 groups. The multi signals in the regions 6.3-6.8 and 7.2-7.8 ppm in the spectrum of the free ligand is assigned to the aromatic protons of benzoyl and naphthoyl rings, respectively [55].

In the ^{1}H-NMR spectra of Cis-[$MoO_2(HTSB)_2$] (Fig. 4 (1)) complexes in d6-DMSO, the disappearance of the OH signal and the greater downfield shift for the CH_3 protons signal at 1.9-2.0 ppm are confirmed participation of the ligands in a bidentate fashion via the OH and the azomethine groups in the coordination to the metal ion. The well-defined multiple signals in the range 7.5-7.3 ppm are close to the multiple signals of the naphthoyl ring.

The ^{1}H-NMR spectral data of the free hydrazone Schiff bases HNEBH, HNEAH, HNE-4\-ABH and their molybdenum (VI) complexes DMSO (δ 2.1 ppm) are summarized in Tables 4.1 and 4.2. The entire Schiff bases showed signals at 2.8, 7.2-8.2 and 11.1 ppm due to methyl proton, ring proton and imine proton (NH), respectively, confirming the existence of the ligands in the keto form [56]. The 1H-NMR spectra of the complexes Cis-[MoO_2(HNEBH)(acac).H_2O] (Fig. 4 (2)) *Cis*-[$Mo_2O_5(HNEAH)_2$] (Fig. 4 (3)) and showed a slight downfield shift of the methyl group signal confirming participation of the azomethine nitrogen of the hydrazone Schiff bases upon coordination with the metal ions [57]. The disappearance of the imine proton signal owing to the apparently deprotonation of the enolic form supports coordination of the azomethine nitrogen and imidic acid oxygen atoms to the metal ions [57]. The HNEBH and HNEAH ligands are coordinated through their monoanionic (NO) - enolate tutomeric form. The multiple signals appeared in the range 3.0-3.1, ppm in the complex *Cis*-[MoO_2(HNEBH)(acac).H_2O] is assigned to the acetylacetone(acac) proton in the coordination sphere. The ^{1}H-NMR spectra of the HNE-4\-ABH hydrazone Schiff base a sharp signal in the range 14.9 ppm and a broad peak in the region 11.6 ppm are observed and are safely attributed to the OH group and NH protons, respectively [42]. In the *Cis*-[MoO_2(HNE-4\-ABH)$_2$.$2H_2O$] complex the broad signal at 15.1 ppm was not changed. These results support the coordination of the Schiff base through the enolic oxygen and azomethine nitrogen, respectively.

The ^{1}H- and ^{13}C-NMR spectra of the chelate *Cis*-[MoO_2(HNENH)(acac)] are summarized in Table 4.3. In the spectra revealed a high field shift of the OH signal and disappearance of –NH- signal suggesting coordination through the enolic oxygen and azomethine nitrogen, respectively [58]. The coordination through the azomethine nitrogen was also confirmed by the observed downfield shift of the –CH_3 signal. The nicotinoyl ring proton signals in the complex ruled out the coordination through the ring nitrogen. The proton-noise decoupled ^{13}C-NMR spectra of Cis-[MoO_2(HNENH)(acac)] complex showed significant downfield shifts of the >C=O and N=C(CH_3) signals supporting the coordination of the carbonyl oxygen and the azomethine nitrogen to the metal ions. Also, Cis-[MoO_2(HNENH)(acac)] complex new signals of acetylacetone (acac) was observed. On the other hand, the nicotinoyl ring carbon signals showed no significant changes suggesting no participation through the ring nitrogen [58].

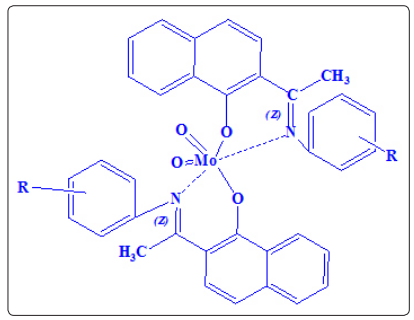

1

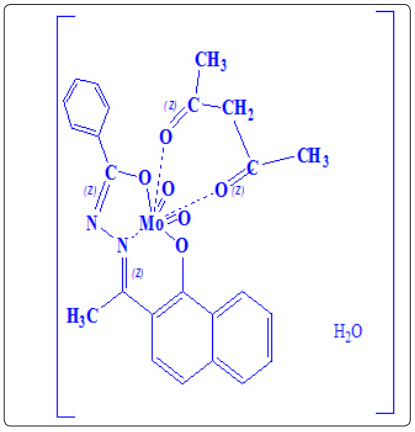

2

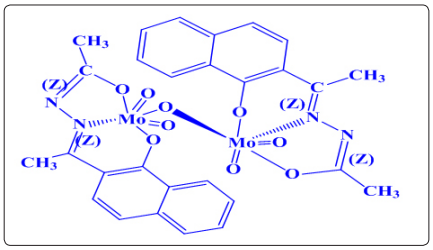

3

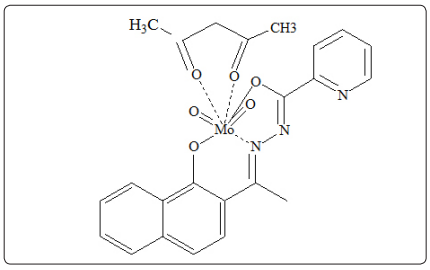

4

Figure 4: The structure of cis- $MoO_2(HRSB)_2$ (1), cis MoO_2(HNEBH)(acac).H_2O (2), cis- $Mo_2O_5(HNEAH)_2$ (3) and cis- MoO_2(HNEPH)(acac) (4) complexes.

Table 4.3 ^{1}H- and ^{13}C-NMR data of Schiff base Hydrazones HNEINH, HNENH, HNEPH and their molybedenum (VI) plexes

Compound	δOH Ppm	δNH	δCH_3	δC=O	δC=N	δpy(C)
HNEINH	11.2(b)	9.8(s)	3.2(s)			
HNENH	11.6(b)	10.1(s)	2.8(s)			
HNEPH	10.7(b)	10.0(s)	2.9(s)	164.4	148.5	123.2-152.4
MoO_2(HNEINH) (acac)	10.8(b)	—	2.4(s)			
MoO_2(HNENH) (acac)	11.6(b)	—	2.3(s)			
MoO_2(HNEPH) (acac)	10.5(b)	—	2.6(s)	168.2	152.4	127.3-156.5

Redox behavior of some Cis-molybdenum(VI) metal complexes

The voltammetric behavior of the complexes *Cis*- $[MoO_2(NE)_2CH_3OH]$ in CH_2Cl_2-TBA+PF6-, *Cis*-$[MoO_2$(HNEINH)(acac)], *Cis*-$[MoO_2$(HNENH)(acac)], and *Cis*-$[MoO_2$(HNEPH)(acac)] in DMF-TBA^+PF6- have been studied by cyclic voltammetry. Voltammetric data are summarized in Table 5 and representative CV is also shown in Fig.5. In the complex Cis-$[MoO_2(NE)_2CH_3OH]$ the cyclic voltammogram displayed one well-defined oxidation wave at +0.6V coupled with one cathodic wave at +0.16 with $E_{1/2}$= +0.38 and ΔE_p=+0.44 V. This electrode reaction is most likely assigned to the irreversible couple Mo^{V}/Mo^{VI}. Another two well defined reduction waves at $E_{p,c}$= -0.14 and -0.6 V coupled with the anodic wave at $E_{p,a}$= -0.02 V are observed and safely assigned to the electrode couples Mo^{V}/Mo^{IV} and Mo^{IV}/Mo^{III} respectively [59].

Table 5 : E_{pa}, E_{pc} are anodic and cathodic peak potentials (V) data vs. Ag/Ag^+ of Cis- molybdenum (VI) complexes

Complex	Oxidation				Reduction				Scan rate mV/S
	E_{pa}	E_{pc}	$E_{1/2}$	ΔE	E_{pa}	E_{pc}	$E_{1/2}$	ΔE	
Cis- $[MoO_2(NE)_2CH_3OH]$	+0.6	+0.16	+0.38	0.44	-0.02	-0.14 -0.6	-0.08	0.12	50
Cis-$[MoO_2$(HNEINH) (acac)]	+0.82 +1.32	+0.12	+o.47	0.7	-0.5	–0.78	-0.64	0.28	50
Cis- $[MoO_2$(HNENH) (acac)],	+0.4 +0.6 +1.1	+0.14	+0.27	0.26	-0.64	-0.88	-0.76	0.24	100
Cis-$[MoO_2$(HNEPH) (acac)]	+0.22 +0.6 +0.8	+0.14 +0.48	+0.18	0.08 0.32	-0. 4	–-1.26	-0.83	0.86	200

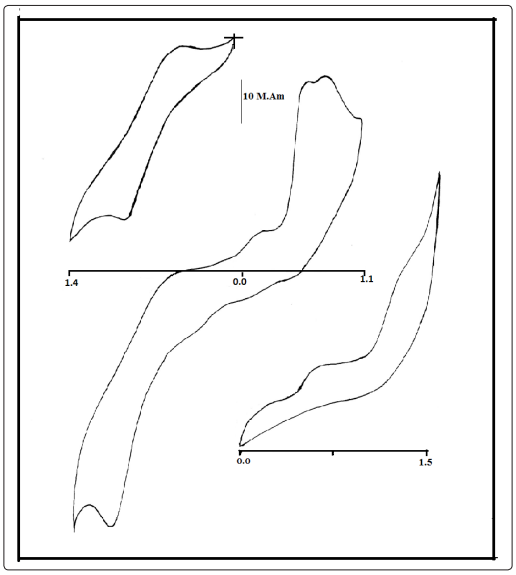

Figure 5: Cyclic voltammograms of the complex *cis*-MoO_2(HNEPH) (acac) at 50 mV/sec scan rate

The observed non-linear relationship between the cathodic peak current, $i_{p,c}$ and the square root of the sweep rate, $v^{1/2}$ (Fig. 6) for the electrode couple Mo^{V}/Mo^{VI} indicates that, the electrochemical process is not diffusion-controlled and a chemically stable product is formed as proposed in scheme 1. Farther, the chemical stability of the observed one-electron reduction product of this complex was also confirmed from the values of the peak current ratio, $i_{p,c}/i_{p,a}$>1 for the reduction process at the different sweep rates used. The peak current parameter $i_{p,c}/v^{1/2}$ of this couple is more or less constant at the employed sweep rates (0.02-0.2 V/sec) and the reverse-to-forward peak current ratios ($i_{p,c}/i_{p,a}$) are close to unity [59]. The one electron nature of this couple has been also established by comparing its peak current heights with other Mo^{V}/Mo^{VI} couples displayed by similar molybdenum (VI) complexes [60-62].

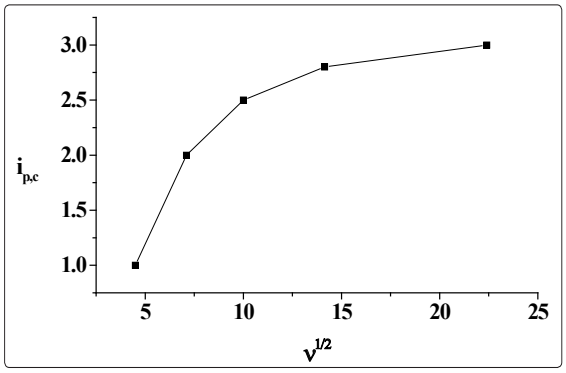

Figure 6: The dependence of the cathodic peak current, $i_{p,c}$ of the electrode couple Mo^{V}/Mo^{VI} of the complex cis-$MoO_2(NE)_2CH_3OH$ upon the scan rate (v)

The CVs of the complexes *Cis*-[MoO_2(HNEINH)(acac)], Cis-[MoO_2(HNENH)(acac)] and *Cis*-[MoO_2(HNEPH)(acac)] showed one reduction and two oxidation waves at 50 mV/sec scan rate. The quasi-reversible one-electron reduction at Ep,c –0.88 V coupled with Ep,a -0.64 V and Scheme *Cis*-[MoO_2(HNEPH)(acac)] displayed one well defined oxidation wave in the range -0.4 — -0.74 V coupled with one cathodic wave at –0.88 — -1.26 V with $E_{1/2}$ in the range –0.68 — -1.0 V. the observed linear relationship between the cathodic peak current and the square root sweep rate ($v^{1/2}$) indicates a diffusion-controlled electrochemical process with one electron reduction to a chemically stable product. Thus, this electrode is mostly likely assigned to the irreversible redox couple Mo^{IV}/Mo^{III} by comparison with other molybdenum(VI) complexes [63,64].

The CV of the complex *Cis*-[MoO_2(HNENH)(acac)] showed two anodic waves in the regions +0.22 and +0.6 V successively coupled with two cathodic waves at +0.14 and +0.48 V with $E_{1/2}$ = 0.18 and 0.54 V, ΔE_p = 0.08 and 0.12 V versus Ag wire electrode. These two couples are safely assigned to the electrode couples Mo^{IV}/Mo^{V} and Mo^{V}/Mo^{VI}, respectively Another anodic wave in the region +0.8—1.32 V is observed at different sweep rates (50-200 mV/sec) and is most likely attributed to the oxidation of the naphtholic hydroxyl group. Similar behaviour was also observed for the complex *Cis*-[MoO_2(HNEPH)(acac)] [65-67].

In the complex *Cis*-[MoO_2(HNEINH)(acac)] the two anodic waves observed at +0.82 and +1.32 V in the couple are assigned to the two electron transfer irreversible process Mo^{V}/Mo^{VI} and oxidation of the naphtholic hydroxy group, respectively [68]. The irreversibility of this peak current was confirmed by the linear dependence of the cathodic peak potential, Ep,c versus log$v$ (Fig. 7). Assuming n=1, an α (electronic transfer coefficient) of 0.62 in the range expected for a single electron transfer [69]. The observed linear relationship between the cathodic peak current $i_{p,c}$ with the square root of sweep rat ($v^{1/2}$) indicates a diffusion-controlled electrochemical process with one electron reduction to a chemically stable product. Thus, this electrode is mostly likely assigned to the electrode couple Mo^{IV}/Mo^{III} by comparison with other molybdenum(VI) complexes.

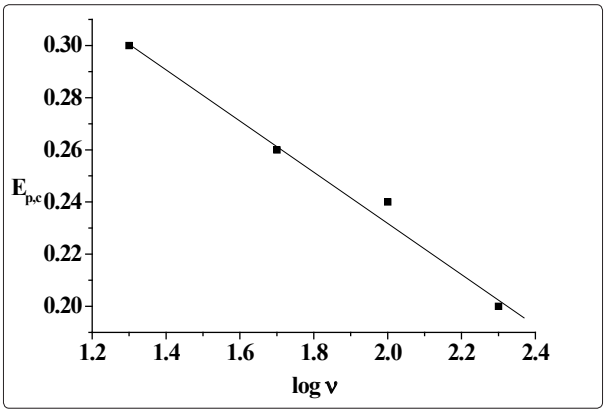

Figure 7: The dependence of the cathodic peak potential, $E_{p,c}$ of the complex *cis*-MoO_2(HNEINH)(acac) on the scan rate (v).

The highest occupied molecular orbital energy levels (E_{HOMO}) of chelating agent HNE, HNEINH, HNENH and HNEPH were calculated using the onset of the oxidation potential with equation (1) [70]. The internal standard was Ferrocene (0.46V vs. Ag/AgCl). The lowest unoccupied molecular orbital energy levels of these ligands (E_{LUMO}) were obtained from equation (2) combined with the optical band gap (Eg) which determined from the band edge of the absorption spectrum (E_g = 1240 / $\lambda_{abs.edge}$) [71]. The results were summarized in Table 6 [71].

Table 6

No.	Compound	λ onset (nm)	E_{ox} onset	E_{HOMO} level (eV)	$E_{Red\ onset}$	ELUMO level (eV)	Eg CV(eV)	Eg (Optical)
1	HNEBH	455	-0.68	-5.08	0.36	-4.04	1.04	2.73
2	HNEAH	460	-0.9	-5.3	0.38	-4.02	1.28	2.70
3	HNEPH	497	-1.2	-5.6	0.42	-3.98	1.62	2.49
4	HNENH	502	-1.0	-5.4	0.1	-4.3	1.1	2.47
5	HNEINH	450	-1.1	-5.5	0.3	-4.1	1.4	2.76
6	HNE-2-ABH	--	-1.26	-5.66	0.28	-4.12	1.54	--
7	HNE-4-ABH	--	-1.0	-5.0	0.34	-4.06	1.34	---
8	HNE	420	-0.82	-5.22	0.8	-3.6	1.62	2.95
9	$MoO_2(NE)_2CH_3OH$	490						2.5
10	MoO_2HNENH(acac)	550						2.3

$E_{HOMO} = -e(E_{1/2(ox.)} - E_{1/2(Fe)} + 4.8)$ (1)
$E_{LUMO} = E_{HOMO} + E_g$ (2)

The E_{HOMO} energy levels of the chelating agents HNE , HNEINH, HNENH and HNEPH were calculated in the range of (-5.0 –(-5.66)) eV and the E_{LUMO} levels were calculated in the range (-3.6 – (-4.12)) eV. The HNEPH exhibit lowest EHOMO levels then the other chelating agents . E_{HOMO} and E_{LUMO} values, frontier orbital energy gap, molecular dipole moment (μ), electron affinity (A), ionization potential (I), electronegativity (χ), global hardness (η), softness (σ), electrophilicity index (ω) and back-donation (ΔE back-donation), were calculated as Koopmans's theorem (Table 7) [72]. The transition of an electron from an E_{HOMO} to an E_{LUMO} level upon photo-excitation at a low unoccupied molecular orbital of the electron acceptor would be collected at the respective electrode. This phenomenon occurred because the excitation binding energy was lower than the electron affinity (A) of the acceptor and the potential difference between the ionization potential (I) of the donor. These properties would estimate the materials were suitable using in photovoltaic devices and solar cells.

Table 7: Molecular dipole moment (μ), frontier orbital energy gap, electron affinity (A), ionization potential (I), electronegativity (χ), global hardness (η), electrophilicity index (ω) and back-donation (ΔE back)

Complexes	μ (Debye)	ΔE_g	A	I	χ	η	ω	S	ΔE_{back}
$MoO_2(NE)_2CH_3OH$	o.47	0.057	0.123	0.18	0.152	0.029	0.038	34.5	$7.13x10^{-3}$
MoO_2HNENH(acac)	0.138	0.259	0.0212	0.28	0.151	0.25	0.038	4	0.0324

Theoretical calculations

In studies of quantum chemistry, the density functional theory (DFT) is an accurate method for the determination of the ground-state wave function and ground –state quantum energy using the Gaussian 09 software. Calculation of the ligands were carried out based on Beck's three parameter exchange functional and Lee–Yang–Parr nonlocal correlation functional (B3LYP) /6-31G(d, p) orbital basis sets for all atoms as implemented [73-76]. Hence, the geometries of *Cis*- [$MoO_2(NE)_2CH_3OH$] and *Cis*-[MoO_2(HNEBH) (acac)] were optimized at the BPV86 [19]. The bond length and bond angles were determined in Table 8, also the electrostatic potential was shown in the Fig. 8- 9.

Table 8: Bond length and bond angle of Cis- [$MoO_2(NE)_2CH_3OH$] complex

Atom	bond length				bond angle		
C(5)							
C(6)	C(5)	1.3370					
C(11)	C(6)	1.3370	C(5)	120.0000			
C(7)	C(6)	1.3370	C(5)	119.9988	C(11)	119.9988	Pro-R
C(10)	C(11)	1.3370	C(6)	120.0000	C(5)	0.0000	Dihedral
C(2)	C(7)	1.3370	C(6)	120.0000	C(5)	-0.0000	Dihedral
C(4)	C(5)	1.3370	C(6)	120.0000	C(7)	0.5729	Dihedral
C(9)	C(10)	1.3370	C(11)	120.0000	C(6)	0.0000	Dihedral
O(15)	C(11)	1.3550	C(6)	115.6990	C(10)	124.2985	Pro-R
C(3)	C(4)	1.3370	C(5)	120.0000	C(6)	0.0000	Dihedral
C(8)	C(5)	1.3370	C(4)	119.9988	C(6)	119.9988	Pro-R
C(13)	C(10)	1.3370	C(9)	119.9988	C(11)	119.9988	Pro-R
Mo(16)	O(15)	1.9400	C(11)	109.5000	C(6)	179.9987	Dihedral
H(40)	C(7)	1.1000	C(2)	120.0000	C(6)	120.0000	Pro-S
Lp(62)	O(15)	0.6000	C(11)	109.4418	Mo(16)	109.4418	Pro-S
Lp(63)	O(15)	0.6000	C(11)	109.4618	Mo(16)	109.4618	Pro-R
N(14)	Mo(16)	1.9760	O(15)	120.0000	C(11)	-0.0006	Dihedral
H(37)	C(2)	1.1000	C(3)	120.0043	C(7)	120.0043	Pro-R
H(38)	C(3)	1.1000	C(2)	120.0050	C(4)	120.0050	Pro-S
H(39)	C(4)	1.1000	C(3)	120.0000	C(5)	120.0000	Pro-R
H(41)	C(8)	1.1000	C(5)	120.0028	C(9)	120.0028	Pro-R
H(42)	C(9)	1.1000	C(8)	120.0016	C(10)	120.0016	Pro-S
C(12)	C(13)	1.4970	C(10)	97.7296	N(14)	97.7296	Pro-R
N(17)	N(14)	1.2480	C(13)	107.5000	Mo(16)	104.0000	Pro-R
O(19)	Mo(16)	1.9400	N(14)	90.0000	O(15)	90.0000	Pro-R
O(26)	Mo(16)	1.6684	N(14)	104.4447	O(15)	79.6000	Pro-S
O(27)	Mo(16)	1.6684	N(14)	147.7431	O(15)	27.7555	Pro-R

O(33)	Mo(16)	1.9400	N(14)	90.0000	O(15)	149.9963	Pro-R
O(34)	Mo(16)	1.9400	N(14)	90.0000	O(15)	90.0000	Pro-R
Lp(61)	N(14)	0.6000	C(13)	124.6623	Mo(16)	127.4683	Pro-S
O(1)	O(27)	7.1309	Mo(16)	174.6233	N(14)	177.9529	Dihedral
C(18)	N(17)	1.2600	N(14)	104.0000	C(13)	-180.0000	Dihedral
C(28)	O(33)	1.2080	Mo(16)	180.0000	N(14)	-128.1204	Dihedral
C(30)	O(34)	1.2080	Mo(16)	180.0000	N(14)	173.4072	Dihedral
H(43)	C(12)	1.1130	C(13)	109.5000	C(10)	-0.0000	Dihedral
Lp(64)	N(17)	0.6000	N(14)	110.7973	C(18)	110.7973	Pro-S
Lp(65)	O(19)	0.6000	Mo(16)	117.4858	C(18)	117.4858	Pro-R
Lp(66)	O(26)	0.6000	Mo(16)	120.0000	N(14)	180.0000	Dihedral
Lp(67)	O(26)	0.6000	Mo(16)	120.0000	N(14)	-0.0000	Dihedral
Lp(68)	O(27)	0.6000	Mo(16)	120.0000	N(14)	-180.0000	Dihedral
Lp(69)	O(27)	0.6000	Mo(16)	120.0000	N(14)	0.0000	Dihedral
Lp(70)	O(33)	0.6000	Mo(16)	65.8047	N(14)	179.3748	Dihedral
Lp(71)	O(33)	0.6000	Mo(16)	20.7157	N(14)	41.4343	Dihedral
Lp(72)	O(34)	0.6000	Mo(16)	89.5226	N(14)	-5.7652	Dihedral
Lp(73)	O(34)	0.6000	Mo(16)	29.4947	N(14)	30.8616	Dihedral
H(35)	O(1)	0.9420	C(5)	59.1977	C(4)	180.0000	Dihedral
Lp(59)	O(1)	0.6000	H(35)	110.8702	C(5)	119.0370	Dihedral
Lp(60)	O(1)	0.6000	H(35)	112.8141	Lp(59)	105.8997	Pro-S
C(21)	C(18)	1.3370	N(17)	154.8737	O(19)	154.8737	Pro-R
C(29)	C(28)	1.5090	O(33)	122.5000	C(5)	-165.8343	Dihedral
H(44)	C(12)	1.1130	C(13)	109.4418	H(43)	109.4418	Pro-S
H(45)	C(12)	1.1130	C(13)	109.4618	H(43)	109.4618	Pro-R
H(36)	O(1)	0.9420	H(35)	103.7000	C(5)	0.0000	Dihedral
C(20)	C(21)	1.3948	C(18)	120.0015	N(17)	-126.8912	Dihedral
C(31)	C(30)	1.5090	C(29)	155.7981	O(34)	155.7981	Pro-S
C(32)	C(28)	1.5090	C(29)	118.7500	O(33)	118.7500	Pro-R
H(51)	C(29)	1.1130	C(28)	123.0143	C(30)	123.0143	Pro-R
H(52)	C(29)	1.1130	C(28)	143.3318	C(30)	143.3318	Pro-S
C(22)	C(20)	1.3948	C(21)	120.0029	C(18)	-179.9942	Dihedral
C(25)	C(21)	1.3949	C(18)	120.0015	C(20)	119.9969	Pro-R
H(53)	C(31)	1.1130	C(30)	109.5000	C(29)	-0.0000	Dihedral
H(56)	C(32)	1.1130	C(28)	109.5000	C(29)	-0.0000	Dihedral
C(23)	C(22)	1.3949	C(20)	119.9996	C(21)	-0.0012	Dihedral
C(24)	C(25)	1.3948	C(21)	120.0002	C(18)	179.9942	Dihedral
H(46)	C(20)	1.1000	C(21)	119.9986	C(22)	119.9986	Pro-S
H(54)	C(31)	1.1130	C(30)	109.4418	H(53)	109.4418	Pro-S
H(55)	C(31)	1.1130	C(30)	109.4618	H(53)	109.4618	Pro-R
H(57)	C(32)	1.1130	C(28)	109.4418	H(56)	109.4418	Pro-S
H(58)	C(32)	1.1130	C(28)	109.4618	H(56)	109.4618	Pro-R
H(47)	C(22)	1.1000	C(20)	120.0002	C(23)	120.0002	Pro-S
H(48)	C(23)	1.1000	C(22)	120.0014	C(24)	120.0014	Pro-S
H(49)	C(24)	1.1000	C(23)	119.9984	C(25)	119.9984	Pro-S
H(50)	C(25)	1.1000	C(21)	119.9999	C(24)	119.9999	Pro-S

Representation data of Mulliken atomic Charges of the complex *Cis*-[$MoO_2(NE)_2.CH_3OH$]:

S. No.	Atoms	Mulliken atomic Charges	S. No.	Atoms	Mulliken atomic Charges
1	C	-0.476609	29	H	0.349813
2	C	0.532270	30	H	0.322921
3	C	-0.388469	31	C	0.138382
4	C	-0.351666	32	C	-0.516102
5	C	-0.566743	33	O	-0.810486
6	C	0.139858	34	C	0.448866
7	C	-0.739914	35	C	-0.741733
8	C	0.425480	36	H	0.342382
9	C	0.098194	37	C	0.133425
10	C	-0.468953	38	C	0.530620
11	H	0.337241	39	C	-0.476401
12	H	0.341753	40	C	-0.564429
13	H	0.332908	41	H	0.322095
14	H	0.347109	42	H	0.346488
15	H	0.322344	43	C	-0.386128
16	H	0.331006	44	C	-0.353695
17	O	-0.804391	45	H	0.330531
18	C	0.730878	46	H	0.333407
19	O	-0.580853	47	Mo	3.943207
20	C	-1.188202	48	O	-1.424958
21	H	0.345327	49	O	-1.456549
22	H	0.346201	50	C	-0.701102
23	H	0.328469	51	H	0.286605
24	H	0.350094	52	H	0.302606
25	H	0.341477	53	O	-0.600515
26	C	-1.193455	54	H	0.317789
27	O	-0.578699	55	H	0.545847
28	C	0.724457			

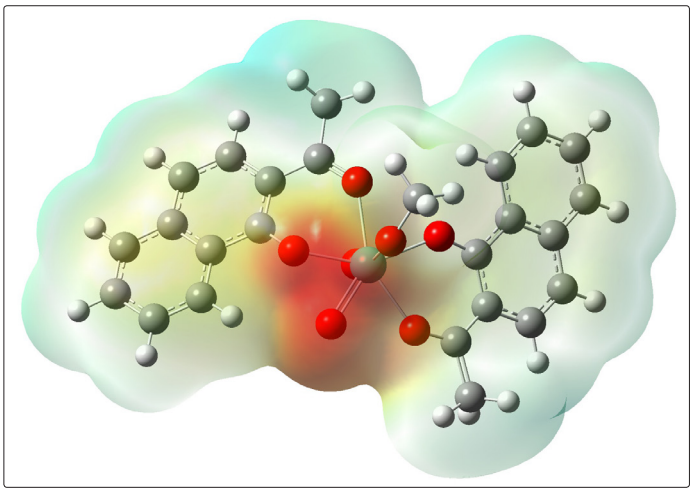

Figure 8: Electron density from total SCF density of *cis*-$MoO_2(NE)_2CH_3OH$ Complex

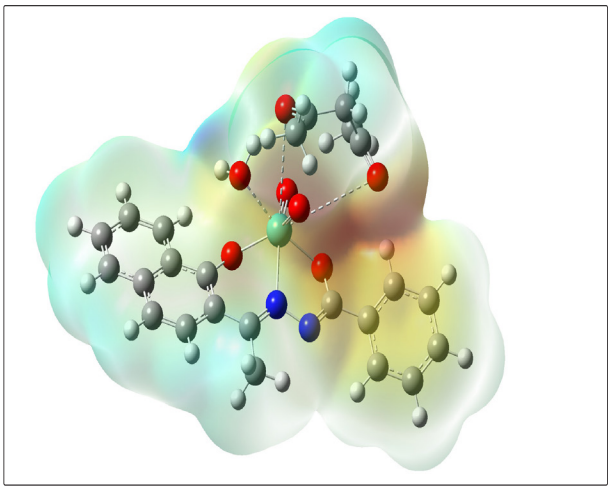

Figure 9: Electron density from total SCF density of *cis*-[$MoO_2(HNEBH)(acac)H_2O$] Complex

Conclusion

A novel molybdenum (VI) complexes have been prepared and fully characterized. The cyclic voltammetry of this complexes indicated that, the Mo^{VI} complexes undergo one or two electron reduction to form the corresponding Mo^{V} or Mo^{IV} complex species. It can be predicted that the dioxo-molybdenum (VI) complexes have the catalytic potential. The $E^{1/2}$ for the couples Mo^{VI}/Mo^{V} and Mo^{V}/Mo^{IV} are very sensitive to the electron-withdrawing or donating properties of the substituent. HOMO and LUMO energy levels have been studied using the UV/vis spectra and energy gap from electrochemical diagram. The molecular dipole moment (μ), electron affinity (A), ionization potential (I), electronegativity (χ), global hardness (η), softness (σ), electrophilicity index (ω) and back-donation (ΔE back-donation) emphasize the chelates have excellent ability to donate electron to the metals. The DFT of the some chelates, and molybdenum complexes shows the activity of complexes.

References

1. Majumder S, Pasayat S, Roy S, Dash SP, Dhaka S, et al. (2018) Dioxidomolybdenum(VI) complexes bearing sterically constrained aroylazine ligands: Synthesis, structural investigation and catalytic evaluation. Inorganica Chim Acta 469: 366-378.
2. Aboafia SA, Elsayed SA, El-Sayed AKA, El-Hendawy AM (2018) New transition metal complexes of 2,4-dihydroxybenzaldehyde benzoylhydrazone Schiff base (H2dhbh): Synthesis, spectroscopic characterization, DNA binding/cleavage and antioxidant activity. J Mol Struct 1158: 39-50.
3. Ram Maurya M, Dogie B, Uprety B, Jangra N, Tomar R, et al. (2018) Oxygen atom transfer between DMSO and benzoin catalyzed by cis–dioxidomolybdenum(VI) complexes of tetradentate Mannich bases.
4. Bagherzadeh M, Mohammadabadi H, Abednatanzi S, Abbasi A, Amini M (2017) Immobilization of a new (salen) molybdenum (VI) complex onto the ion-exchangeable polysiloxane as a heterogeneous epoxidation catalyst. Nanochemistry Res 2: 179-187.
5. Cui YM, Qiao L, Li Y, Wang Q, Chen W, et al. (2017) Synthesis, crystal structures and catalytic epoxidation properties of dioxomolybdenum (VI) complexes with hydrazone ligands. Transit Met Chem 42: 51-56.
6. Peng DL (2016) Two dioxomolybdenum (VI) complexes with hydrazone ligands: synthesis, characterization, crystal structures and catalytic properties. Transit Met Chem 41: 843-848.
7. Roy S, Dash SP, Acharyya R, Kaminsky W, Ugone V, et al. (2018) Chemistry of oxidomolybdenum (IV) and-(VI) complexes with ONS donor ligands: Synthesis, computational evaluation and oxo-transfer reactions, Polyhedron 141: 322-336.
8. Roy S, Saswati S Lima, Dhaka S, Maurya MR, Acharyya R, et al. (2018) Synthesis, structural studies and catalytic activity of a series of dioxidomolybdenum(VI)-thiosemicarbazone complexes. Inorganica Chim Acta 474: 134-143.
9. Hermes-Lima M, Gonçalves MS, Andrade RG (2001) Pyridoxal isonicotinoyl hydrazone (PIH) prevents copper-mediated in vitro free radical formation. Mol Cell Biochem 228: 73-82.
10. Easmon J, Heinisch G, Pürstinger G, Langer T, Österreicher JK, et al. (1997) Azinyl and diazinyl hydrazones derived from aryl N-heteroaryl ketones: synthesis and antiproliferative activity. J Med Chem 40: 4420-4425.
11. Mostafa MM, Khattab MA, Ibrahim KM (1983) Metal complexes of schiff's base derived from salicoylhydrazine and biacetylmonoxime Polyhedron 2: 583-585.
12. El-Hendawy AM, El-Kourashy AEG, Shanab MM (1992) Schiff base complexes of ruthenium(III), molybdenum(VI) and uranium(VI), and use of the former as catalytic organic oxidants. Polyhedron 11: 523-530.
13. Pasayat S, Dash SP, Roy S, Dinda R, Dhaka S, et al. (2014) Synthesis, structural studies and catalytic activity of dioxidomolybdenum (VI) complexes with aroylhydrazones of naphthol-derivative. Polyhedron 67: 1-10.
14. Maurya RC, Vishwakarma PK, Mir JM, Rajak DK (2016) Oxidoperoxidomolybdenum (VI) complexes involving 4-formyl-3-methyl-1-phenyl-2-pyrazoline-5-one and some β-diketoenolates. J Therm Anal Calorim 124: 57-70.
15. Magalon A, Fedor JG, Walburger A, Weiner JH (2011) Molybdenum enzymes in bacteria and their maturation. Coord Chem Rev 255: 1159-1178.
16. Chen GJJ, McDonald JW, Newton WE (1976) Synthesis of molybdenum(IV) and molybdenum(V) complexes using oxo abstraction by phosphines. Mechanistic implications. Inorg Chem 15: 2612-2615.
17. Vogel AI (2013) A Text-Book Of Quantitative Inorganic Analysis-Theory And Practice, Longmans, Green And Co.; London; New York; Toronto.
18. Sayin K, Karakaş D (2018) Quantum chemical investigation of levofloxacin-boron complexes: A computational approach. J Mol Struct 1158: 57-65.
19. Bühl M, Reimann C, Pantazis DA, Bredow T, Neese F (2008) Geometries of third-row transition-metal complexes from density-functional theory. J Chem Theory Comput 4: 1449-1459.
20. Vogel AI (1959) Elementary practical organic chemistry, Longmans, Green.
21. El-Hendawy AM, Griffith WP, Pumphrey CA (1988) Complexes of osmium, uranium, molybdenum, and tungsten with the catechol amines adrenaline, noradrenaline, dopamine, dopa, and isoproterenol. J Chem Soc Dalt Trans 1817-1821.
22. Geary WJ (1971) The use of conductivity measurements in organic solvents for the characterisation of coordination compounds. Coord Chem Rev 7: 81-122.
23. Catalan J, del Valle JC (1993) Toward the photostability mechanism of intramolecular hydrogen bond systems. The photophysics of 1'-hydroxy-2'-acetonaphthone. J Am Chem Soc 115: 4321-4325.
24. El-Hendawy AM, El-Shahawi MS (1989) Complexes of ruthenium(III) derived from O,O-donor ligands. Polyhedron 8: 2813-2816.
25. Nielson AJ, Griffith WP (1978) Complexes of osmium (VI) with catechol and substituted catechols. J Chem Soc Dalt Trans 1501-1506.
26. Yamada K (1962) Infrared and ultraviolet spectra of α-and γ-pyrones. Bull Chem Soc Jpn 35: 1323-1329.
27. Ferraro JR (2012) Low-frequency vibrations of inorganic and coordination compounds, Springer Science & Business Media.
28. Finnegan MM, Lutz TG, Nelson WO, Smith A, Orvig C (1987) Neutral water-soluble post-transition-metal chelate complexes of medical interest: aluminum and gallium tris (3-hydroxy-4-pyronates). Inorg Chem 26: 2171-2176.
29. Baker AW, Shulgin AT (1959) Intramolecular hydrogen bonding. II. The determination of Hammett sigma constants

by intramolecular hydrogen bonding in Schiff's bases. J Am Chem Soc 81: 1523-1529.
30. Freedman HH (1961) Intramolecular H-bonds. I. A spectroscopic study of the hydrogen bond between hydroxyl and nitrogen. J Am Chem Soc 83: 2900-2905.
31. Kovacic JE (1967) The C- N stretching frequency in the infrared spectra of Schiff's base complexes—I. Copper complexes of salicylidene anilines, Spectrochim. Acta Part A Mol Spectrosc 23: 183-187.
32. Sellmann D, Nakamoto K (1971) Infrared Spectra of Inorganic and Coordination Compounds. John Wiley & Sons. New York, London, Sydney, Toronto, 1970. 338 Seiten, zahlreiche Abbildungen und Tabellen. Preis: 140s, Berichte Der Bunsengesellschaft Für Phys Chemie 75: 603-604.
33. Teyssie P, Charette JJ (1963) Physico-chemical properties of co-ordinating compounds—III: Infra-red spectra of N-salicyclidenealkylamines and their chelates. Spectrochim Acta 19: 1407-1423.
34. Liu X, Manzur C, Novoa N, Celedón S, Carrillo D, et al. (2018) Multidentate unsymmetrically-substituted Schiff bases and their metal complexes: Synthesis, functional materials properties, and applications to catalysis. Coord Chem Rev 357: 144-172.
35. Henry RP, Mitchell PCH, Prue JE (1973) Hydrolysis of the oxovanadium (IV) ion and the stability of its complexes with the 1, 2-dihydroxybenzenato (2–) ion. J Chem Soc Dalt Trans 1156-1159.
36. Mahmoud MR, El-Haty MT (1980) Co (II), Ni (II), Cu (II), Th (IV), and U (VI) Complexes of some Heterocyclic Schiff bases derived from Hydroxy Aromatic aldehydes and 2-Aminopyridine. J Inorg Nucl Chem 42: 349-353.
37. Geetharani K, Sathyanarayana DN (1977) Metal complexes of thiosemicarbazide: Vibrational analysis of nickel (II) thiosemicarbazide complexes and their deutero isotopomers. Aust J Chem 30: 1617-1624.
38. Sathyanarayana DN, Nicholls D (1978) Vibrational spectra of transition metal complexes of hydrazine. Normal coordinate analyses of hydrazine and hydrazine-d4. Spectrochim Acta Part A Mol Spectrosc 34: 263-267.
39. D Hall (1965) A refinement of the structure of formamidoxime. Acta Crystallogr 18: 955-958.
40. Fabian WMF, Antonov L, Nedeltcheva D, Kamounah FS, Taylor PJ (2004) Tautomerism in hydroxynaphthaldehyde anils and azo analogues: a combined experimental and computational study. J Phys Chem A 108: 7603-7612.
41. Biradar NS, Patil BR, Kulkarni VH (1975) Transformation of square-planar dsp2 configuration of Ni (II) aldoximates into octahedral sp3d2 configuration by reaction with tin (IV) chloride. J Inorg Nucl Chem 37: 1901-1904.
42. Nawar N, Hosny NM (2000) Synthesis, spectral and antimicrobial activity studies of o-aminoacetophenone o-hydroxybenzoylhydrazone complexes. Transit Met Chem 25: 1-8.
43. Li L, Lopes PS, Rosa V, Figueira CA, Lemos MANDA, et al. (2012) Synthesis and structural characterisation of (aryl-BIAN) copper(i) complexes and their application as catalysts for the cycloaddition of azides and alkynesElectronic supplementary information (ESI) available: tables containing: electrochemical data for the 41: 5144-5154.
44. Sahni SK, Sangal SK, Gupta SP, Rana VB (1977) Some 5-coordinate nickel (II) complexes of dipicolinic acid hydrazide. J Inorg Nucl Chem 39: 1098-1100.
45. Sakamoto M (1987) Synthesis and characterization of lanthanoid (III) complexes with a pentadentate ligand derived from 2, 6-diacetylpyridine and benzoylhydrazide. Inorganica Chim Acta 131: 139-142.
46. Garg BS, Kurup MRP, Jain SK, Bhoon YK (1988) Spectroscopic studies on copper (II) complexes derived from a substituted 2-acetylpyridine thiosemicarbazone. Transit Met Chem 13: 309-312.
47. Jones LH (1959) Determination of UO bond distance in uranyl complexes from their infrared spectra. Spectrochim Acta 15: 409-411.
48. Ueno K, Martell AE (1956) Infrared Studies on Synthetic Oxygen Carriers. J Phys Chem 60: 1270-1275.
49. Dziembowska T, Rozwadowski Z, Filarowski A, Hansen PE (2001) NMR study of proton transfer equilibrium in Schiff bases derived from 2-hydroxy-1-naphthaldehyde and 1-hydroxy-2-acetonaphthone. Deuterium isotope effects on 13C and 15N chemical shifts. Magn Reson Chem 39: S67-S80.
50. Organero JA, Douhal A (2003) Temperature and solvent effects on the photodynamics of 1′-hydroxy-2′-acetonaphthone. Chem Phys Lett 381: 759-765.
51. Syamal A, Maurya MR (1986) Synthesis and characterization of nickel (II), cobalt (II), copper (II), manganese (II), zinc (II), zirconium (IV), dioxouranium (VI) and dioxomolybdenum (VI) complexes of a new Schiff base derived from salicylaldehyde and 5-methylpyrazole-3-carbohydrazid. Transit Met Chem 11: 172-176.
52. Mostafa SI (1998) Complexes of 2-hydroxynaphthalene-1-carboxaldehyde with transition metal ions. Transit Met Chem 23: 397-401.
53. Teotia MP, Gurtu JN, Rana VB (1980) Dimeric 5-and 6-coordinate complexes of tri and tetradentate ligands. J Inorg Nucl Chem 42: 821-831.
54. Jha NK, Joshi DM (1985) Synthesis and characterization of triorganoantimony (V) complexes with bidentate ligands. Polyhedron 4: 2083-2087.
55. Becker ED (1980) High resolution NMR: theory and chemical applications, Elsevier.
56. Becker ED (1980) High Resolution NMR 2nd edit.
57. Narang KK, Singh VP (1993) Synthesis and characterization of cobalt (II), nickel (II), copper (II) and zinc (II) complexes with acetylacetone bis-benzoylhydrazone and acetylacetone bis-isonicotinoylhydrazone. Transit Met Chem 18: 287-290.
58. Paolucci G, Marangoni G, Bandoli G, Clemente DA (1980) Reactivity of uranyl ion with quinquedentate chelating hydrazine derivatives. Part 2. 2, 6-Diacetylpyridine bis (4-methoxybenzoylhydrazone). J Chem Soc Dalt Trans 1304-1311.
59. Charney LM, Finklea HO, Schultz FA (1982) Electrochemistry, spectroelectrochemistry, and electron paramagnetic resonance spectroscopy of aqueous molybdenum (VI),-(V),-(IV), and-(III) catechol complexes. Stabilization of reduced monomers in weakly alkaline solution. Inorg Chem 21: 549-556.
60. Lynch WE, Lintvedt RL, Shui XQ (1991) Osmium (VI)-dioxo complexes derived from. beta.-diketone Schiff bases and their reactivity with arene-and alkanethiols. Synthesis, characterization, structures, and electrochemical data. Inorg Chem 30: 1014-1019.
61. Al-Saif FA, Alibrahim KA, Alosaimi EH, Assirey E, El-Shahawi MS, et al. (2018) Synthesis, spectroscopic and electrochemical characterizations of new Schiff base chelator towards Ru3+,

Pt4+ and Ir3+ metal ions. J Mol Liq 266: 242-251.
62. Cinquantini A, Seeber R, Cini R, Zanello P (1982) Voltammetric behaviour of transition metal complexes with extended-systems schiff base ligands: N, N′-ethylenebis (acetylacetoniminato) palladium (II), copper (II) and nickel (II) complexes. J Electroanal Chem Interfacial Electrochem 134: 65-73.
63. Bard AJ, Faulkner LR (2001) Fundamentals and applications. Electrochem Methods 2: 482.
64. Rajan OA, Chakravorty A (1981) Molybdenum complexes. 1. Acceptor behavior and related properties of Mo (VI) O_2 (tridentate) systems. Inorg Chem 20: 660-664.
65. Purohit S, Koley AP, Prasad LS, Manoharan PT, Ghosh S (1989) Chemistry of molybdenum with hard-soft donor ligands. 2. Molybdenum (VI),-(V), and-(IV) oxo complexes with tridentate Schiff base ligands. Inorg Chem 28: 3735-3742.
66. Lal RA, Kumar A, Chakraborty J, Bhaumik S (2001) Molybdenum (VI),(V) and (IV) complexes with chiral benzoin thiosemicarbazone. Transit Met Chem 26: 557-562.
67. Mafatle TJ, Nyokong T (1996) Electrocatalytic oxidation of cysteine by molybdenum (V) phthalocyanine complexes. J Electroanal Chem 408: 213-218.
68. Nocera DG, Gray HB (1984) Electrochemical reduction of molybdenum (II) and tungsten (II) halide cluster ions. Electrogenerated chemiluminescence of tetradecachlorohexamolybdate (2-) ion. J Am Chem Soc 106: 824-825.
69. Dinoi C, Guedes da Silva MFC, Alegria ECBA, Smoleński P, Martins LM, et al. (2010) Molybdenum Complexes Bearing the Tris (1-pyrazolyl) methanesulfonate Ligand: Synthesis, Characterization and Electrochemical Behaviour. Eur J Inorg Chem 2010: 2415-2424.
70. Lin M, Li D, Wang X, Luo C, Ling Q (2016) Synthesis and optical properties of white phosphorescent carbazole - iridium copolymers. J Macromol Sci Part A 53: 222-226.
71. Shafiee A, Salleh MM, Yahaya M (2011) Determination of HOMO and LUMO of [6, 6]-phenyl C61-butyric acid 3-ethylthiophene ester and poly (3-octyl-thiophene-2, 5-diyl) through voltametry characterization. Sains Malaysiana 40: 173-176.
72. Koopmans T (1934) Über die Zuordnung von Wellenfunktionen und Eigenwerten zu den einzelnen Elektronen eines Atoms. Physica 1: 104-113.
73. Karzazi Y, Belghiti ME, El-Hajjaji F, Boudra S, Hammouti B (2016) Density functional theory modeling and monte carlo simulation assessment of inhibition performance of two quinoxaline derivatives for steel corrosion. J Mater Environ Sci 7: 4011-4023.
74. Stephens PJ, Devlin FJ, Chabalowski CFN, Frisch MJ (1994) Ab initio calculation of vibrational absorption and circular dichroism spectra using density functional force fields. J Phys Chem 98: 11623-11627.
75. Devlin FJ, Finley JW, Stephens PJ, Frisch MJ (1995) Ab initio calculation of vibrational absorption and circular dichroism spectra using density functional force fields: a comparison of local, nonlocal, and hybrid density functionals. J Phys Chem 99: 16883-16902.
76. J Sworakowski (2018) How accurate are energies of HOMO and LUMO levels in small-molecule organic semiconductors determined from cyclic voltammetry or optical spectroscopy?. Synth Met 235: 125-130.